Temporal upscaling of evapotranspiration for drip-irrigated grapevines in solar greenhouses: A comparative study in Northeast China's cold region

Jingjing Zhao[1,2], Xinguang Wei[2*], Senyan Jiang[2]

(1. *School of Petrochemical Engineering, Liaoning Petrochemical University, Fushun 113001, Liaoning, China*;
2. *College of Water Conservancy, Shenyang Agricultural University, Shenyang 110866, China*)

Abstract: Temporal upscaling of evapotranspiration (ET) is crucial for improving water use efficiency and water-saving irrigation management in crop production, playing a vital role in guiding farmland irrigation. This study investigated the water consumption patterns and evaluated different temporal upscaling methods for ET in drip irrigated grapevines in Northeast China's cold region. Based on a three-year experiment (2018, 2020, 2021), four upscaling methods were examined: the evaporation fraction method (EF method), the improved evaporation fraction method (EF′ method), the crop coefficient method (K_c method), and the direct canopy resistance method (r_c method), applied to both instantaneous-to-daily and daily-to-whole-growth-period timescales. The results demonstrated that all key parameters, including evaporation fraction (EF), improved evaporation fraction (EF′), crop coefficient (K_c), and canopy resistance (r_c), exhibited stable values from 8:00-16:00 when upscaling ET from instantaneous to daily scales. Their mean standard deviations (SD) ranged from 0.08-0.21, 0.08-0.19, 0.10-0.18, and 41.43-137.72 s/m, respectively. Regarding the simulation of instantaneous to daily upscaling, the methods ranked as EF method>EF′ method>K_c method>r_c method. The EF method achieved optimal performance at specific times: 11:30 (shoot growth and the flowering period), 12:00 (fruit expansion), and 12:30 (maturity). For daily to whole growth period upscaling, all four methods performed best during the fruit expansion stage, maintaining the same performance ranking. The EF method consistently exhibited the smallest errors, with MAE values of 35.31 mm, 33.00 mm, and 42.97 mm, and RRMSE values of 12.21%, 11.40%, and 14.62% in 2018, 2020, and 2021, respectively. Therefore, the EF method is recommended for both upscaling ET from instantaneous to daily timescales and from daily to the entire growth period for drip-irrigated grapevines in Northeast China's cold region. The findings not only enrich the analytical framework for agricultural hydrological processes, but also hold significant implications for implementing "hourly precision water management" in greenhouse grape cultivation and enhancing water use efficiency in greenhouse grape systems.

Keywords: evapotranspiration, methods for temporal upscaling, improved evaporation fraction, crop coefficient, greenhouse grapevines

DOI: 10.25165/j.ijabe.20261903.9948

Citation: Zhao J J, Wei X G, Jiang S Y. Temporal upscaling of evapotranspiration for drip-irrigated grapevines in solar greenhouses: A comparative study in Northeast China's cold region. Int J Agric & Biol Eng, 2026; 19(3): 294–306.

1 Introduction

Evapotranspiration (ET) is a crucial component of agricultural water balance and a key link in the soil-plant-atmosphere continuum[1], playing a pivotal role in irrigation water management[2-4]. Understanding the characteristics of ET variations at different timescales is essential. These timescale effects enable the transformation of ET across spatial and temporal scales, supporting scientific irrigation planning and improved water use efficiency[5-7]. By 2018, China's facility agriculture cultivation area reached 1.89×10^6 hm^2, accounting for 82% (2.29×10^6 hm^2) of the global total[8].

In the semi-enclosed cultivation environment of a greenhouse, irrigation is the sole source of water for crop growth, making the evapotranspiration (ET) process of greenhouse grapes highly susceptible to irrigation practices. Furthermore, the unique light-transmitting structure of the irregular front roof, along with the complex insulation and heat storage-release facilities, significantly alter the water-heat transfer processes within the greenhouse. Consequently, ET in greenhouses is typically characterized by high humidity and weak convection. Its process is not only more complex than that of field crops but also exhibits strong spatial and temporal heterogeneity. On the other hand, ET at larger temporal scales is not a simple accumulation of small-scale observations; a complex nonlinear relationship exists between them. Traditional ET upscaling methods, which are suitable for field crops, cannot be directly applied to greenhouse conditions. Therefore, in-depth research on relevant upscaling methods tailored to greenhouse environments is urgently needed. Numerous studies have shown that the ET transformation at large scales is not a simple linear superposition of small scales, and there is a complex nonlinear relationship between them[4,9,10]. Accurate temporal scaling of different time scales of ET transformations and understanding their time-scale effects are critical for greenhouse crop water management[11,12]. The main common methods for ET upscaling are the evaporation fraction method (EF method), improved evaporation fraction method (EF′ method), crop coefficient method (K_c method), direct canopy resistance method (r_c method), and sine method[13]. Shuttleworth et al.[14] defined the ratio of latent heat flux to available energy as evaporation fraction (EF). Sugita &

Received date: 2025-06-03 **Accepted date:** 2026-04-09

Biographies: Jingjing Zhao, PhD, research interest: utilization of bio-resource, Email: jingjing6180@126.com; **Senyan Jiang**, PhD, research interest: water-saving irrigation, Email: Jsy573@163.com.

***Corresponding author: Xinguang Wei**, PhD, Associate Professor, research interest: efficient use of water for greenhouse crops. College of Water Conservancy, Shenyang Agricultural University, Shenyang 110866, China. Tel: +86-15710504925, Email: weixg@syau.edu.cn.

Brutsaert[15] found that EF usually varies very little during daytime, which established the theoretical basis for using instantaneous available energy and EF to estimate daily ET. This method formed the evaporation fraction method. Chemin et al.[16] assumed that the soil heat flux (G) in the evaporation fraction has a mean value of approximately zero during daytime, so G can be ignored to reduce the error due to its uncertainty, leading to the improved evaporation fraction method of ET upscaling. Farah et al.[17] analyzed the daytime variation of canopy resistance (r_c) and proposed a method that can estimate daily ET based on r_c, establishing the direct canopy resistance method, which reverses r_c by the Penman-Monteith equation, and shows that r_c is approximately constant during daytime[18]. Allen et al.[1] found that the ratio of instantaneous ET to reference crop evapotranspiration (ET_0), termed the crop coefficient (K_c), was almost constant during daytime and could be used as an upscaling method for ET, forming the crop coefficient method. Tang et al.[19] demonstrated that in the crop coefficient method, the assumption of constant canopy resistance during daytime for ET_0 is not consistent with the actual crop canopy resistance variation pattern, which is affected by solar radiation, saturated water vapor deficit, and wind speed, leading to the crop coefficient method being improved by using the changing canopy resistance, resulting in the improved crop coefficient method. Jackson et al.[9] found that there is a sine relationship between daily solar radiation and instantaneous daytime solar radiation on sunny days, and the ratio of daily ET to instantaneous daytime ET can be replaced by the ratio of daily solar radiation and instantaneous daytime solar radiation, enabling the instantaneous ET to be scaled to daily ET, establishing the sine method.

Numerous studies have explored methods for temporal upscaling of evapotranspiration (ET)[20,21]. Yan et al.[22] evaluated multiple methods for tea and winter wheat in Jiangsu, finding that the EF and EF′ methods performed best for instantaneous-to-daily upscaling, particularly between 12:00 and 14:00. Colaizzi[13] conducted research on alfalfa, cotton, and sorghum in Texas, USA, and showed that both the EF and K_c methods could reliably estimate daily ET, with the optimal estimation period being 12:40-14:15; under crop cover conditions, the K_c method performed slightly better, but Yang et al.[23] pointed out that this method may be unreliable when there are large deviations in ET_0 calculations. Li et al.[12] studied rice paddies in Jiangsu and found that the EF method exhibited the best consistency across all daytime periods. Chen et al.[24] compared multiple crops including winter wheat, summer maize, and sorghum in the North China Plain and Northeast Plain, and found that the sine method showed systematic overestimation, while the EF, EF′, and K_c methods performed best during the 12:00-13:00 period, with the EF′ method showing the best overall performance. Jiang et al.[25] evaluated the applicability of six methods across six ecosystem types and found that the EF′ method had the broadest applicability; the optimal simulation periods for each method varied by ecosystem and method, but were generally concentrated between 12:00 and 15:00. Nassar et al.[26] studied grapevines in California, USA, and showed that the EF method outperformed the sine method. Zhang et al.[27] researched summer maize in North China and showed that the EF and K_c methods performed best at 13:00, while other methods performed best around 12:00. Liu et al.[28] found that the K_c method was suitable for estimating ET from daily to entire growth period scales for winter wheat in North China. The optimal simulation timing and accuracy of ET temporal upscaling methods vary with environmental conditions and crop types, and the performance of the same method differs across ecosystems, growth stages, and time periods[29-31]. However, the applicability of these methods under greenhouse cultivation conditions has not yet been reported.

Therefore, this study was conducted with the following objectives: 1) To examine the characteristics of ET changes in greenhouse grapevines at different time scales; 2) To determine the optimal upscaling time and evaluate the accuracy of four instantaneous and daily methods; 3) To assess the applicability of different ET temporal upscaling methods for grapevines under greenhouse growing conditions in northeastern cold regions, aiming to determine the best upscaling method and provide a scientific basis for moisture management of grapes in northeastern greenhouses.

2 Materials and methods

2.1 Study sites

The experiment was carried out in 2018-2021 in Solar Greenhouse No. 44 of the Scientific Research Experiment Base of Shenyang Agricultural University, located in Northeast China (123.57°E, 41.82°N, 82 m above sea level). Due to damage to the data collection equipment in 2019, substantial data was missing, so this study only used the data of 2018, 2020, and 2021. The greenhouse was of the Chinese Liao Shen III solar energy-saving type (CLSSG-III)[32], with an east-west orientation, a span of 8 m, a ridge height of 4 m, and a length of 60 m. The arched steel frame served as the front roof support and was covered with a 0.15 mm PO film. Greenhouse temperature was regulated through automatically controlled top and bottom vents, each with a maximum opening of 150 cm, adjusted dynamically based on thermal requirements.

The experimental greenhouse consisted of 111 five-year-old *Muscat Hamburg* vines (planted in 2016) arranged in 0.5 m (within-row)×4.7 m (between-row) spacing. Drip irrigation was employed, with a drip head flow rate of 2 L/h and uniformly arranged drip emitters. The irrigation thresholds were set at 90% (upper limit) and 60% (lower limit) of field water capacity (θ_f, cm^3/cm^3). In 2018, 2020, and 2021, the total irrigation volumes were 357 mm, 347 mm, and 363 mm, respectively. Fertilizer application rates were N-P_2O_5-K_2O at 260-119-485 kg/hm^2. The experimental soil was a medium loam with a targeted wet layer depth of 60 cm. The 0-60 cm soil had a bulk density of 1.44 g/cm^3 and a field water capacity of 0.32 cm^3/cm^3. Other standard agronomic management practices such as pruning and pest control followed local solar greenhouse grape production guidelines. Following the method employed in previous vineyard studies[33,34], the grapevine growing season was divided into four distinct phenological stages: the shoot growth stage (stage Ⅰ), flowering and fruit setting stage (stage Ⅱ), fruit expansion stage (stage Ⅲ), and maturity stage (stage Ⅳ). The specific temporal durations for each phenological stage are presented in Figure 1 and Figure 2.

2.2 Monitoring indicators

Meteorological data collection: A microclimate monitoring system was deployed within the greenhouse, equipped with the following sensors and corresponding parameters: a temperature and relative humidity sensor (HMP155A, Vaisala, Finland) for air temperature (T_a, °C) and relative humidity (RH, %); a net radiation sensor (LPNET07, Delta Ohm, Italy) for net radiation (R_n, W/m^2); a sonic anemometer (CSAT3, Campbell Scientific, USA) for wind speed (u, m/s); and soil heat flux plates (HFP01, Hukseflux, Netherlands) installed at a depth of 5 cm for soil heat flux. These parameters were recorded annually from April 1 to September 30 during 2018–2021 using a CR1000 data logger (Campbell Scientific, USA) at a sampling interval of 10 min. Due to substantial data gaps in 2019, the analysis was limited to the datasets from 2018, 2020, and 2021.

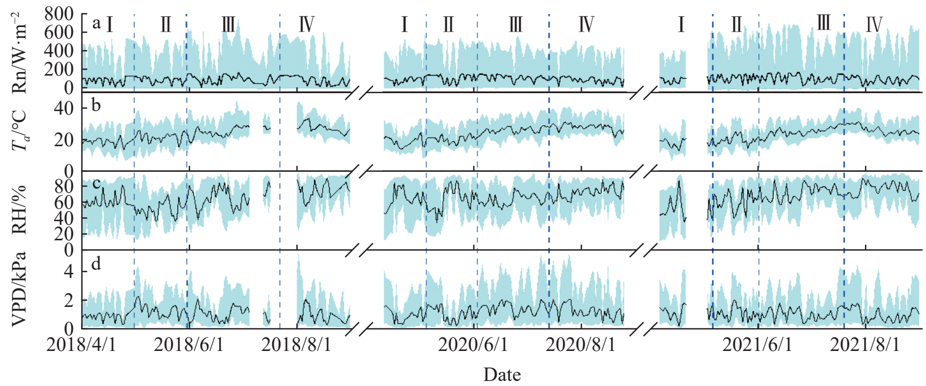

Note: Rn is net radiation, T_a is air temperature, RH is relative humidity, VPD is vapor pressure deficit. The blue area represents the diurnal fluctuation range, and the solid line represents the intraday average. Ⅰ, Ⅱ, Ⅲ, Ⅳ represent the shoot growth stage, flowering and fruit setting stage, fruit expansion stage, and maturity stage, respectively.

Figure 1 Dynamic variations in meteorological factors

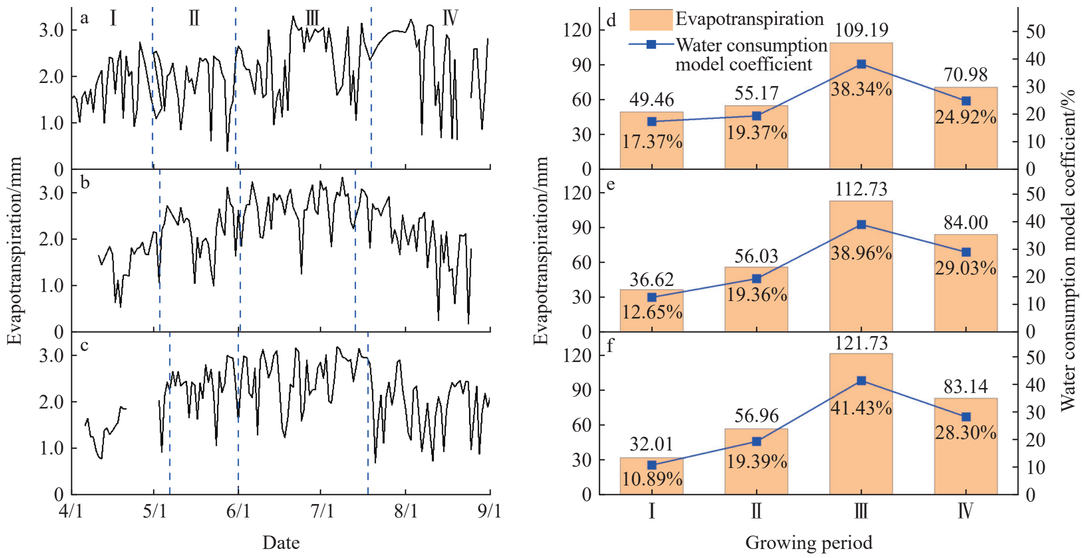

Note: Symbols Ⅰ, Ⅱ, Ⅲ, and Ⅳ represent the shoot growth stage, flowering and fruit setting stage, fruit expansion stage, and maturity stage, respectively. Figures 2a-2c show daily variations of evapotranspiration for the years 2018, 2020, and 2021, respectively. Figures 2d-2f show the water consumption model coefficient for the years 2018, 2020, and 2021, respectively.

Figure 2 Daily variations of evapotranspiration and water consumption model coefficient across growth stages

Sap flow measurements: Five grapevines were selected, and their sap flow dynamics (F) were monitored continuously (Flow32-1K, Dynamax, USA) throughout the entire growth period using a wraparound sap flow measurement system. Sensors were installed approximately 20 cm above the base of the vine trunk, and data were collected by the CR1000 data acquisition system at 10-min intervals. Because the soil surface was fully covered with plastic mulch, soil evaporation was considered to be negligible[35,36], and grapevine transpiration assumed equal to evapotranspiration (ET). ET was calculated following the equation provided by Zheng et al.[37]:

$$F_t = \frac{P_{in} - Q_r - Q_v}{C_p - \Delta T} \tag{1}$$

where, F_t is the instantaneous sap flow rate at time t, g/h; P_{in} is the heat input, fixed at 0.2 W; Q_r is the radial heat dissipation, W; Q_v is the vertical heat conduction, which is offset by a pair of symmetrical thermocouples and thus considered 0 W; C_p is the specific heat of water, 4.186 J/(g·°C); and ΔT is the average value of the sum of voltages from the two vertical thermocouples, °C.

The equations for daily and entire growth period ET of grapevines were calculated as follows[38]:

$$\mathrm{ET_{id}} = \int_0^{1440} F_{it}\mathrm{d}t \frac{3600A_{is}}{1000A_i} \tag{2}$$

$$\mathrm{ET}_d = \sum_{i=1}^{5} \mathrm{ET_{id}}/5 \tag{3}$$

$$\mathrm{ET}_p = \sum_{k=1}^{n} \mathrm{ET}_d \tag{4}$$

where, $\mathrm{ET_{id}}$ is the daily evapotranspiration of the i-th test grape plant, mm; A_{is} is the cross-sectional area of the water-conducting part of the trunk for the i-th test grape plant, cm^2; A is the sample area, m^2; ET_p is the ET of the entire growth period, mm; n is the No. of day number in the entire growth period, d.

2.3 ET upscaling methods

2.3.1 Evaporation fraction method

The evaporation fraction (EF) is defined as the ratio of the latent heat flux (λE) to the available energy (Rn-G). The ET temporal upscaling method based on EF can be expressed as follows[14,15]:

1) Instantaneous to daily ET.

$$\mathrm{EF}_i=\frac{\lambda\mathrm{ET}_i}{(\mathrm{Rn}-G)_i} \tag{5}$$

$$\lambda\mathrm{ET}_d=\mathrm{EF}_i(\mathrm{Rn}-G)_d \tag{6}$$

2) Daily to entire growth period ET.

$$\mathrm{EF}_d=\frac{\lambda\mathrm{ET}_d}{(\mathrm{Rn}-G)_d} \tag{7}$$

$$\lambda\mathrm{ET}_p=\sum_{k=1}^{n}[\mathrm{EF}_d\times(\mathrm{Rn}-G)_{\mathrm{dk}}] \tag{8}$$

where, EF_i is the instantaneous evaporation fraction, and EF_d is the daily evaporation fraction. $\lambda\mathrm{ET}_i$, $\lambda\mathrm{ET}_d$, and $\lambda\mathrm{ET}_p$ are the latent heat flux at time i, total daytime, and entire growth period, respectively, W/m^2, and λ is the latent heat of vaporization, J/kg. Rn is the net radiation, W/m^2, and G is the soil heat flux, W/m^2. The subscripts i and d express a certain instantaneous time and total daytime values, respectively. n is the number of entire growth period days, d.

2.3.2 Improved evaporation fraction method

Soil heat flux (G) can be approximated as zero on a daily scale[26], so the G term in Equations (5)-(8) can be ignored. The improved evaporation fraction method is:

1) Instantaneous to daily ET.

$$\mathrm{EF}_i'=\frac{\lambda\mathrm{ET}_i}{\mathrm{Rn}} \tag{9}$$

$$\lambda\mathrm{ET}_d=\mathrm{EF}_i'\mathrm{Rn}_d \tag{10}$$

2) Daily to entire growth period ET.

$$\mathrm{EF}_d'=\frac{\lambda\mathrm{ET}_d}{\mathrm{Rn}_d} \tag{11}$$

$$\lambda\mathrm{ET}_p=\sum_{k=1}^{n}\left[\mathrm{EF}_{\mathrm{dk}}'\times\mathrm{Rn}_{\mathrm{dk}}\right] \tag{12}$$

where EF_i' is the improved evaporation fraction, and EF_d' is the daily improved evaporation fraction.

2.3.3 Crop coefficient method

Crop coefficient (K_c) is defined as the ratio of ET to the reference ET_0, and the K_c method is formulated as follows[39]:

1) Instantaneous to daily ET.

$$\lambda\mathrm{ET}_{0i}=\frac{\Delta_i(R_n-G)_i+\dfrac{\rho_{ai}C_p\mathrm{VPD}_i u_{2i}}{208}}{\Delta_i+\gamma_i(1+0.34u_{2i})} \tag{13}$$

$$\lambda\mathrm{ET}_{0d}=\frac{\Delta_d(R_n-G)_d+\dfrac{\rho_{ad}C_p\mathrm{VPD}_d u_{2d}}{208}}{\Delta_d+\gamma_d(1+0.34u_{2d})} \tag{14}$$

$$K_{ci}=\frac{\lambda\mathrm{ET}_i}{\lambda\mathrm{ET}_{0i}} \tag{15}$$

$$\lambda\mathrm{ET}_d=K_{\mathrm{ci}}\lambda\mathrm{ET}_{0d} \tag{16}$$

2) Daily to entire growth period ET.

$$K_{\mathrm{cd}}=\frac{\lambda\mathrm{ET}_d}{\lambda\mathrm{ET}_{0d}} \tag{17}$$

$$\lambda\mathrm{ET}_p=\sum_{k=1}^{n}[\mathrm{K}_{\mathrm{cdk}}\times\lambda ET_{0\mathrm{dk}}] \tag{18}$$

where K_{ci} is the instantaneous crop coefficient; K_{cd} is the daily crop coefficient in k growth stage; K_{cdk} is the average crop coefficient of growth stage k; $\lambda\mathrm{ET}_0$ is the latent heat flux from the reference crops, W/m^2; $\lambda\mathrm{ET}_d$ is the daily latent heat flux of grapevine, W/m^2; $\lambda\mathrm{ET}_p$ is the grapevine latent heat flux of entire growth period, W/m^2. Δ is the slope of the saturation vapor pressure curves, kPa/°C; ρ_{a} is the air density, kg/m^3; C_p is the specific heat of dry air at constant pressure, J/(kg·K); VPD is the vapor pressure deficit, kPa, respectively. γ is the psychrometric constant, kPa/°C. u_2 is the wind speed at 2 m height, m/s. The subscripts i and d express a certain instantaneous time and total daytime values, respectively.

2.3.4 Direct canopy resistance method

The ET temporal upscaling method based on canopy resistance r_c is as follows[40]:

$$r_c=\frac{\rho_a C_p}{2h_s\mathrm{LAI}} \tag{19}$$

where, ρ_{a} is the air density, kg/m^3; C_p is the specific heat of moist air at constant pressure, MJ/(kg·°C); h_s is the heat transfer coefficient, which has been modified for solar greenhouse conditions; details of the modification are provided in Zheng et al.[41].

1) Instantaneous to daily ET.

$$r_{\mathrm{ci}}=r_{\mathrm{ai}}\left[\left(\frac{\Delta_i(\mathrm{Rn}-G)_i+\dfrac{\rho_{\mathrm{ai}}C_p\mathrm{VPD}_i}{r_{\mathrm{ai}}}}{\lambda\mathrm{ET}_i}-\Delta_i\right)\frac{1}{\gamma_i}-1\right] \tag{20}$$

$$\lambda\mathrm{ET}_{\mathrm{d}}=\frac{\Delta_d(\mathrm{Rn}-G)_d+\dfrac{\rho_{\mathrm{ad}}C_p\mathrm{VPD}_d}{r_{\mathrm{ad}}}}{\Delta_d+\gamma_d\left(1+\dfrac{r_{\mathrm{ci}}}{r_{\mathrm{ad}}}\right)} \tag{21}$$

2) Daily to entire growth period ET.

$$r_{\mathrm{cd}}=r_{\mathrm{ad}}\left[\left(\frac{\Delta_d(\mathrm{Rn}-G)_d+\dfrac{\rho_{\mathrm{ad}}C_p\mathrm{VPD}_d}{r_{\mathrm{ad}}}}{\lambda\mathrm{ET}_{\mathrm{d}}}-\Delta_d\right)\frac{1}{\gamma_d}-1\right] \tag{22}$$

$$\lambda\mathrm{ET}_p=\sum_{k=1}^{n}\frac{\Delta_{\mathrm{dk}}(\mathrm{Rn}-G)_{\mathrm{dk}}+\dfrac{\rho_{\mathrm{adk}}C_p\mathrm{VPD}_{\mathrm{dk}}}{r_{\mathrm{adk}}}}{\Delta_{\mathrm{dk}}+\gamma_{\mathrm{dk}}\left(1+\dfrac{r_{\mathrm{cdk}}}{r_{\mathrm{adk}}}\right)} \tag{23}$$

where, r_{ci} is the instantaneous canopy resistance, s/m, and r_{cd} is daily canopy resistance, s/m; r_{ai} is the aerodynamic resistance, s/m. z is the height of wind measurements, m; d is the zero-plane displacement height, m; z_0 is the roughness length governing momentum transfer, m; z_{0h} is the roughness length governing transfer of heat and vapor, m. u_z is the wind speed at height z, m/s. The subscripts i and d express a certain instantaneous time and total daytime values, respectively. k is the von Kármán constant.

2.4 Evaluation of method performance

The coefficient of determination (R^2), relative root mean square error (RRMSE), efficiency coefficient (ε), mean absolute error (MAE), and global performance indicator (GPI) were used to evaluate the simulation effects of each ET method, which were calculated as follows[25,42]:

$$R^2 = \frac{\left[\sum (X_i - \bar{X})(Y_i - \bar{Y})\right]^2}{\sum (X_i - \bar{X})^2 \sum (Y_i - \bar{Y})^2} \tag{24}$$

$$\text{RRMSE} = \frac{\sqrt{\sum \frac{1}{N}(X_i - Y_i)^2}}{\bar{X}} \tag{25}$$

$$\varepsilon = 1 - \frac{\sum |X_i - Y_i|}{\sum (X_i - Y_i)^2} \tag{26}$$

$$\text{MAE} = \frac{\sum |X_i - Y_i|}{N} \tag{27}$$

$$\text{GPI} = \sum \left[\alpha(\bar{O}_j - O_j\right] \tag{28}$$

where, X_i is the observed value; Y_i is the simulated value; N is the sample number; $\bar{X}_j$ is the mean of the observed values; $\bar{Y}$ is the mean of the simulated values; O_j is the normalized value of the above three evaluation indicators; and $\bar{O}_j$ is the median of each index after normalization. When j is RRMSE and MAE, α=1, and when it is R^2 and ε, α=–1; the higher GPI values indicate a better overall simulation effect of the method. *R* software was used for data analysis, and Origin software was used for graphing.

3 Results

3.1 Environmental conditions

The characteristics of the three-year variation of environmental factors in the solar greenhouse are shown in Figure 1. Net radiation (Rn) in 2018, 2020, and 2021 showed an overall unimodal trend throughout the entire grapevine growth stage, with the daily maximum Rn occurring at the fruit expansion period, reaching 170 W/m² (June 29), 153 W/m² (June 14), and 164 W/m² (June 24) in the three years, respectively. Air temperature (T_a) showed an overall unimodal trend during the entire growth period, varying between 6.6°C-46.6°C, 8.3°C-40.9°C, and 6.4°C-40.0°C in the 3 a, with mean values of 23.3°C, 24.0°C, and 23.3°C, respectively. Relative humidity (RH) varied between 13.0% and 97.0%, 12.5% and 97.6%, and 11.8% and 97.2% in the 3 a, with mean values of 63.2%, 66.6%, and 68.1%, respectively. Vapor pressure deficit (VPD) varied between 0.1 and 5.2 kPa, 0.1 and 5.3 kPa, and 0.1 and 4.4 kPa in the 3 a.

3.2 Daily evapotranspiration and consumption model coefficient in each growth stage of grapevines

The diurnal patterns and daily ET characteristics of greenhouse grapevines for the 3 a are shown in Figure 2 and Figure 3. The total ET values were 284.80 mm, 289.38 mm, and 293.84 mm in 2018, 2020, and 2021, respectively. The water consumption model coefficient is a key indicator reflecting the proportion of water consumption during each growth stage of the crop. In this study, this coefficient was found to be the highest during the fruit expansion stage across all 3 a, with values of 38.34%, 38.96%, and 41.43% in 2018, 2020, and 2021, respectively. Over the 3 a study period, the ranking of this coefficient across growth stages remained consistent: fruit expansion stage>maturity stage>flowering and fruit setting stage>shoot growth stage. From Figure 3, the daily peak of sap flow rate occurred between 11:00 and 14:00, and the start and stop times were basically the same (within ±30 min) across all growth stages. Figure 3 shows peak sap flow rates were 237-265, 295-306, 338-344, and 304-314 g/h during the shoot growth, flowering and fruit setting, fruit expansion, and maturity stages, respectively.

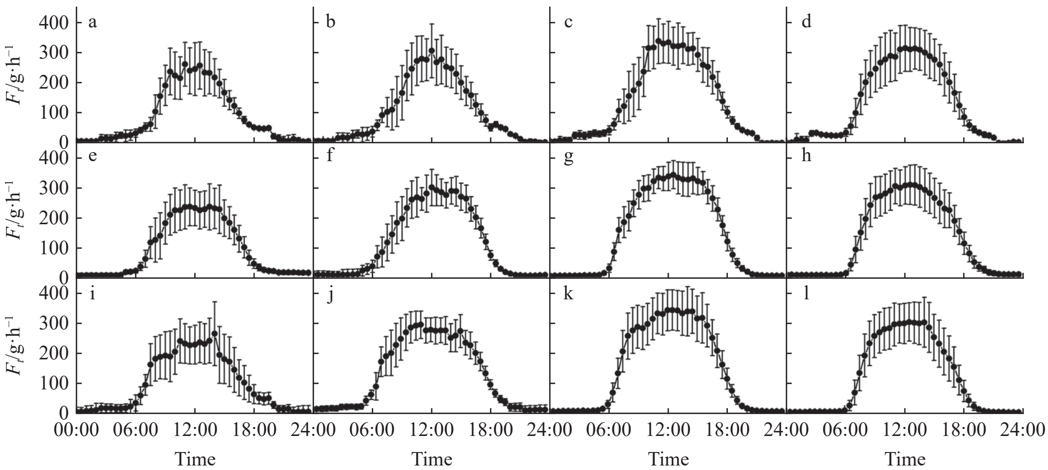

Note: Figures 3a-3d, 3e-3h, and 3i-3l represent the shoot growth stage, flowering and fruit setting period, fruit expansion period, and maturity stage for the years 2018, 2020, and 2021, respectively.

Figure 3 Diurnal dynamics of sap flow rate (F_t) across four growth stages

3.3 Key parameters for temporal upscaling

Figure 4 presents the diurnal patterns and daily dynamics of critical parameters (EF, EF′, K_c, and r_c) derived through four temporal upscaling methodologies. Diurnal dynamics of key parameters (EF, EF′, K_c, and r_c) exhibited consistent U-shaped patterns in Figures 4a-4d, with stabilization phases occurring during 08:00 to 16:00. During the 2018 growing season, measured ranges from 06:00 to 18:00 were 0.46-0.73, 0.47-0.71, 0.62-1.25, and 191.0-275.3 s/m for EF, EF′, K_c, and r_c respectively, accompanied by standard deviations of 0.08-0.19, 0.08-0.22, 0.12-0.27, and 58.3-191.5 s/m. The 8:00-16:00 window demonstrated minimized variability, with mean standard deviations of 0.11, 0.10, 0.16, and 91.0 s/m for respective parameters representing significant reductions (5.8% to 19.5%) compared to 24 h baselines across the 3 a data set. These characteristics substantiate the selection of 8:00-16:00 observations for temporal upscaling of ET fluxes.

3.4 Instantaneous to daily ET upscaling

The model performance metrics of four temporal upscaling methodologies (EF, EF ′, K_c, and r_c method) for greenhouse grapevine evapotranspiration estimation were systematically evaluated through R^2, RRMSE, ε, and MAE indices, as detailed in Figures 5-8.

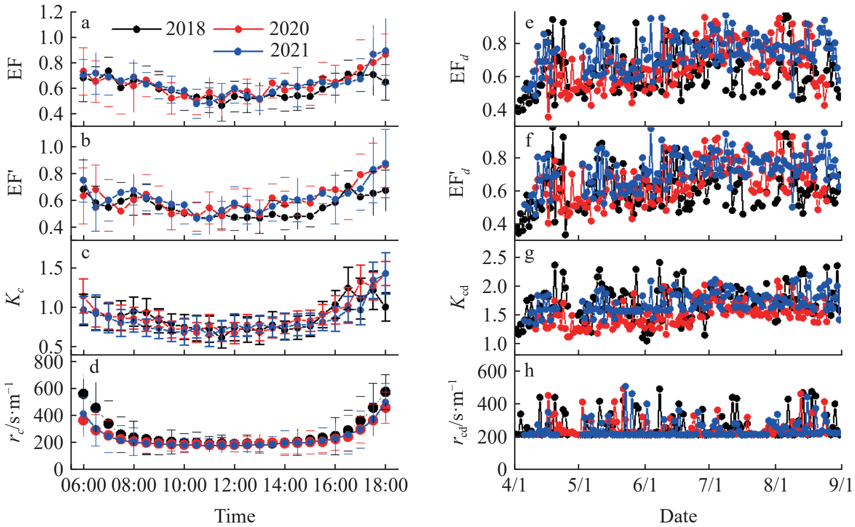

Note: Figures 4a-4d represent the evaporation fraction (EF), modified evaporation fraction (EF′), crop coefficient (K_c), and direct canopy resistance (r_c), respectively. Figures 4e-4h represent the daily evaporation fraction (EF$_d$), daily improved evaporation fraction (EF′$_d$), daily crop coefficient (K_{cd}), and daily direct canopy resistance (r_{cd}), respectively.

Figure 4 Dynamic changes of key parameters in 2018, 2020, and 2021

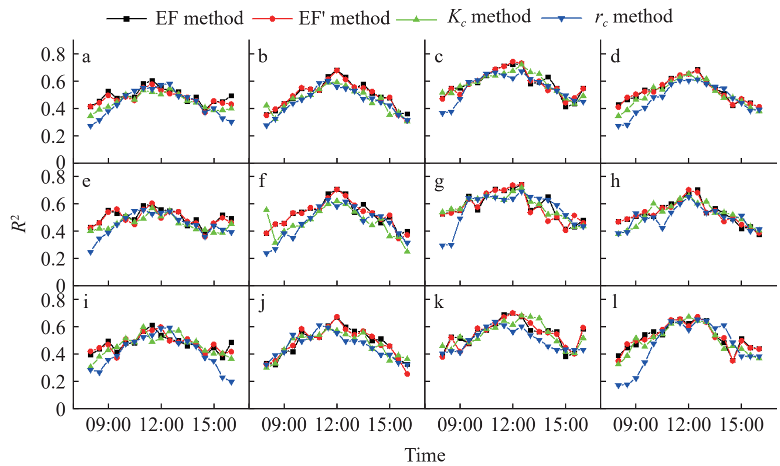

Note: Figures 5a-5d, 5e-5h, and 5i-5l represent the R^2 of shoot growth stage, flowering and fruit setting stage, fruit expansion stage, and maturity stage for the years 2018, 2020, and 2021, respectively.

Figure 5 Variations in coefficient of determination (R^2) of daily evapotranspiration

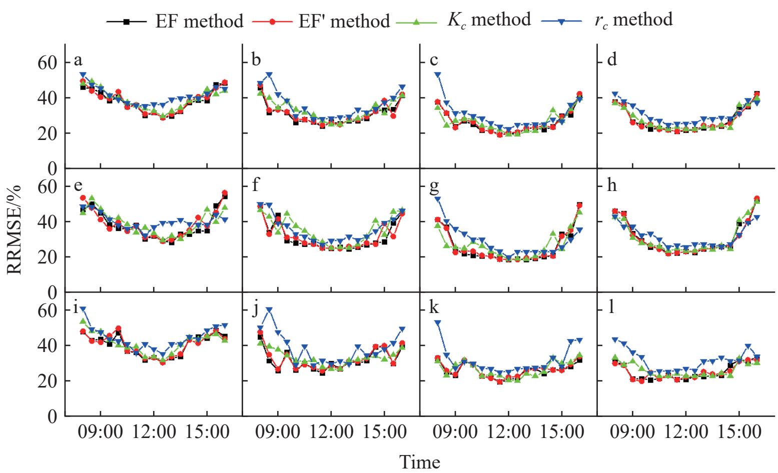

Note: Figures 6a-6d, 6e-6h, and 6i-6l represent the shoot growth stage, flowering and fruit setting stage, fruit expansion stage, and maturity stage for the years 2018, 2020, and 2021, respectively.

Figure 6 Variations in daily relative root mean square error (RRMSE)

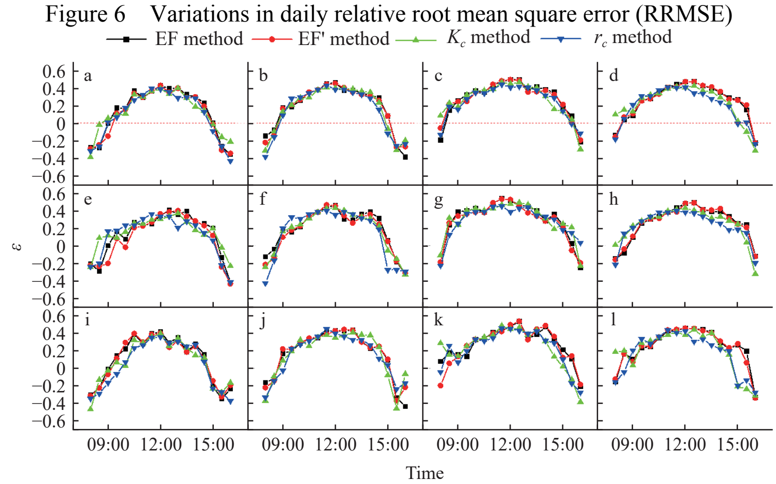

Note: Figures 7a-7d, 7e-7h, and 7i-7l represent the shoot growth stage, flowering and fruit setting stage, fruit expansion stage, and maturity stage for the years 2018, 2020, and 2021, respectively.

Figure 7 Variations in efficiency coefficient (ε) of daily evapotranspiration

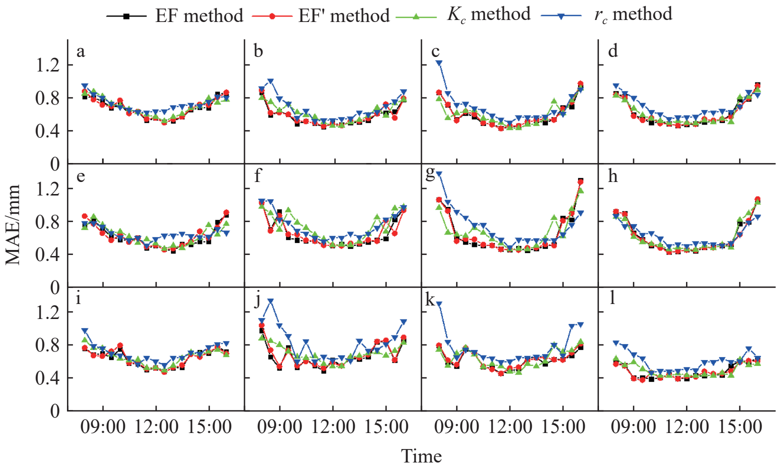

Note: Figures 8a-8d, 8e-8h, and 8i-8l represent the shoot growth stage, flowering and fruit setting stage, fruit expansion stage, and maturity stage for the years 2018, 2020, and 2021, respectively.

Figure 8 Variations in mean absolute error (MAE) of daily evapotranspiration

Figure 5 demonstrates that the four temporal upscaling methodologies (EF, EF′, K_c, r_c) exhibited consistent inverted U-shaped trajectories in R^2 dynamics across three consecutive growing seasons (2018, 2020, and 2021). During phenological progression in 2018, daily mean R^2 values progressively increased from shoot growth phase (EF=0.49, EF′=0.47, K_c=0.45, r_c=0.44) to a peak during the fruit expansion stage (EF=0.59, EF′=0.59, K_c=0.58, r_c=0.55), followed by gradual decline during maturity stage (EF=0.53, EF′=0.53, K_c=0.50, r_c=0.48). This pattern persisted through 2020 and 2021 (interannual R^2 variation <±5%), with method-specific performance divergence: EF method dominated in 2018 (R^2=0.60) and 2021 (R^2=0.62), while EF′ method performed best in 2020 (R^2=0.61), suggesting that parameter efficacy was modulated by microenvironmental factors (VPD range: 0.8-2.3 kPa).

Figure 6 demonstrates that the four methodologies exhibited phenological-stage-specific U-shaped RRMSE patterns over growing seasons in 2018, 2020, and 2021. During 2018's shoot growth phase, daily mean RRMSE values reached 37.98% (EF), 38.46% (EF′), 39.27% (K_c), and 41.16(r_c), with analogous trends (r^2=0.85-0.91) observed during flowering and fruit setting and fruit expansion stages. Maturity phase data showed interannual consistency (2018: EF=37.98%, EF′=38.46%, K_c=39.27%, r_c=41.16%; 2020: ±1.2% variation), while 2021 exhibited shifted methodological hierarchy (EF>EF′>K_c>r_c; Kendall's W=0.87). Critical analysis reveals minimum RRMSE occurred consistently during fruit expansion (EF: 19.15% in 2018, 18.33% in 2020, and 19.50% in 2021), contrasting with shoot growth stage performance where EF′ dominated in 2018 (28.62%) and 2021 (30.31%), versus EF's superiority in 2020 (28.13%). This interannual variability (ΔRRMSE=2.8%-4.1%) underscores microenvironmental regulation (VPD fluctuations: 1.2-3.4 kPa) on methodology efficacy.

Figure 7 reveals that the four methodologies exhibited phenologically synchronized inverted U-shaped ε trajectories inversely correlated with RRMSE patterns across the 3 a. During shoot growth phases, mean daily ε demonstrated significant interannual discrepancies (CV=25%-38%): EF: 0.14 (2018), 0.13 (2020), 0.11 (2021); EF′ (0.11, 0.10, 0.11); K_c (0.13, 0.15, 0.08); r_c (0.10, 0.12, 0.05) in 2018, 2020, and 2021. Flowering and fruit setting stage showed progressive ε escalation, with 2018 values peaking at 0.19 (EF), 0.18 (EF′), 0.17 (K_c), 0.15 (r_c); a pattern maintained in 2020 (with a variation of less than ±0.02), while 2021 values moderated to 0.17, 0.18, 0.16, 0.15 respectively. The highest ε values occurred during fruit expansion (2018: EF=0.28, EF′=0.28,

K_c=0.27, r_c=0.25; 2020 to 2021: ±0.03 variation), where daily peaks reached 0.55 (EF), 0.54 (EF′), 0.50 (K_c), 0.46 (r_c). Interannual maximum variations emerged across phenological stages: EF climaxed at 0.46 during 2018 flowering, EF′ at 0.47 (2020), and K_c at 0.45 (2021), reflecting microenvironmental regulation on parameter sensitivity.

Figure 8 illustrates phenological-stage-dependent U-shaped MAE trajectories across methodologies, exhibiting strong interannual consistency. During 2018's shoot growth phase, daily mean MAE values measured 0.67 mm (EF), 0.68 mm (EF′), 0.69 mm (K_c), and 0.73 mm (r_c), with analogous patterns (R^2=0.89-0.93) persisting through flowering and fruit setting and fruit expansion stages. Maturity phase analysis revealed methodological hierarchy stability in 2018 (EF=0.60 mm, EF′=0.61 mm, K_c= 0.62 mm, r_c=0.69 mm) and 2020, contrasting with 2021's distinct performance gradient (EF>EF′>K_c>r_c). Minimal MAE values demonstrated microenvironmental sensitivity: EF′ achieved 0.50 mm (2018) and 0.48 mm (2021) during shoot growth, while EF dominated in 2020 (0.44 mm, CV=12.3%), reflecting VPD-modulated parameter efficacy variations across growing seasons.

Comparative analysis of four temporal upscaling methodologies across multiple validation metrics (R^2, RRMSE, ε, MAE) demonstrated metric-dependent performance variability under interannual (2018 to 2021) and phenological stage-specific conditions. During the 2018 maturity phase, EF method achieved peak R^2 (0.53±0.04), while EF′ exhibited superior multi-metric optimization (RRMSE=27.23%, ε=0.26, MAE=0.60 mm), which revealed parameter-specific sensitivity to microclimatic drivers (VPD=1.6 to 2.8 kPa). Optimal temporal windows clustered around solar noon (11:00 to 13:30 Local Standard Time, LST), though metric-specific optima shifted significantly (ΔT=±45 minutes; R^2=0.76-0.88 between metrics), necessitating multi-criteria decision analysis (MCDA) for robust temporal optimization.

3.5 The optimal time window for instantaneous to daily ET upscaling

The global performance indicator (GPI) contrast of different growing stages in 2018, 2020, and 2021 is listed in Table 1. As shown in the table, the optimal upscaling moments varied by method and growth stage: for the EF method, they occurred at 11:30 (shoot growth stage, GPI=1.57), 11:30 (flowering and fruit setting period, GPI=0.95), 12:00 (fruit expansion period, GPI=1.00), and 12:30 (maturity stage, GPI=0.98); for the EF′ method, at 11:30 (GP=1.63), 12:00 (GPI=0.99), 12:00 (GPI=1.03), and 12:30 (GPI=1.10) for the respective growth stages; for the K_c method, at 12:30 (GPI=1.75), 12:00 (GPI=1.32), 12:30 (GPI=1.19), and 12:00 (GPI=0.96); and for the r_c method, at 11:30 (GPI=1.03), 11:30 (GPI=1.03), 12:30 (GPI=0.62), and 11:00 (GPI=0.92) across the four growth stages.

Table 1 Global performance indicator contrast of different growing stages in 2018, 2020, and 2021

Time	Shoot growth stage				Flowering and fruit setting stage				Fruit swelling stage				Mature period			
	EF	EF′	K_c	r_c	EF	EF′	K_c	r_c	EF	EF′	K_c	r_c	EF	EF′	K_c	r_c
8:00	–1.77	–1.80	–2.02	–2.71	–2.61	–2.71	–2.25	–2.57	–2.21	–2.31	–1.48	–3.17	–2.29	–2.26	–2.12	–2.90
8:30	–1.51	–1.07	–1.47	–1.87	–1.15	–1.22	–2.03	–2.52	–1.03	–1.05	–0.36	–1.57	–1.74	–1.56	–1.61	–2.05
9:00	–0.59	–0.34	–0.96	–1.08	–0.86	–0.70	–0.79	–1.12	–0.24	–0.39	–0.50	–0.92	–0.70	–0.48	–0.89	–1.26
9:30	–0.13	–0.11	–0.24	–0.40	–0.58	–0.40	–0.88	–0.48	–0.37	–0.46	–0.34	–0.34	–0.13	0.04	–0.25	–0.58
10:00	–0.26	–0.30	0.18	0.20	0.27	0.21	–0.19	0.31	–0.09	–0.17	–0.29	–0.02	0.12	–0.05	0.27	0.08
10:30	0.51	0.66	0.54	0.62	0.20	0.32	0.07	0.13	0.36	0.37	0.29	0.19	0.28	0.50	0.37	0.31
11:00	0.77	0.93	1.04	0.94	0.34	0.44	0.48	0.94	0.64	0.70	0.40	0.48	0.66	0.77	0.74	0.92
11:30	1.57	1.63	1.23	1.03	0.95	0.92	1.07	1.03	0.99	0.99	0.69	0.63	0.86	0.98	0.75	0.89
12:00	1.24	1.43	1.30	1.01	0.88	0.99	1.32	0.83	1.00	1.03	0.99	0.61	0.91	0.99	0.96	0.89
12:30	1.37	1.50	1.75	1.01	0.73	0.83	1.20	0.73	0.95	0.97	1.19	0.62	0.98	1.10	0.87	0.78
13:00	1.27	1.34	1.33	0.33	0.34	0.37	0.79	0.62	0.14	0.15	0.74	0.43	0.48	0.45	0.65	0.39
13:30	0.58	0.91	0.77	0.24	0.36	0.30	0.60	0.09	0.12	0.12	0.65	0.28	0.26	0.32	0.46	0.27
14:00	0.18	0.27	0.18	0.04	0.03	0.05	–0.01	0.17	0.32	–0.18	–0.07	0.06	–0.01	0.02	–0.01	0.09
14:30	–0.48	–0.53	–0.18	–0.33	–0.50	–0.43	–0.58	–0.22	–0.12	–0.13	–1.22	–0.26	–0.70	–0.46	0.09	–0.15
15:00	–0.45	–0.35	–1.03	–0.78	–0.80	–1.16	–0.89	–0.92	–1.30	–1.19	–0.87	–0.56	–1.29	–0.83	–1.74	–0.87
15:30	–1.74	–1.31	–0.93	–1.67	–1.59	–1.24	–2.03	–1.51	–1.47	–1.59	–1.77	–1.54	–1.49	–1.56	–2.11	–1.86
16:00	–1.75	–1.72	–1.14	–1.85	–2.47	–2.43	–2.39	–2.10	–2.51	–2.51	–2.62	–1.97	–2.92	–2.80	–2.89	–2.07

Table 1 shows the multi-criteria performance evaluation across phenological stages in 2018, 2020, and 2021, revealing methodology-specific temporal optimization patterns. EF method achieved peak efficiency at 11:30 LST (shoot growth: GP=1.57± 0.05), maintaining midday optimization through flowering and fruit setting (11:30 LST, GPI=0.95) and fruit expansion (12:00 LST, GPI=1.00), shifting to 12:30 LST (maturity: GPI=0.98). EF′ demonstrated progressive phase-delayed optimization (11:30 to 12:30 LST) with ascending GPI values (1.63 to 1.10), while K_c and r_c methodologies exhibited divergent hierarchical patterns: K_c peaked earlier (12:00 LST, GPI=1.32) during flowering versus r_c's delayed optimization (12:30 LST, GPI=1.19). Greenhouse specific methodologies showed distinct diurnal preferences, with solar noon alignment (12:30 LST, GPI=0.62±0.08) in expansion stages, and contrasting with optimization time advance (11:00 LST, GPI=0.92) during maturity stages.

Figure 9 and Table 2 present the multi-method ET upscaling performance at methodology-specific optimal temporal windows, which demonstrates high precise alignment across phenological stages (NRMSE<12%). Regression analyses revealed systematic method biases: EF and EF′ methods consistently underestimated daily ET (MBE=–0.23±0.05 mm), while K_c and r_c methods exhibited periodic overestimation (MAE=+0.18±0.07 mm) during canopy senescence phases (LAI<3.0). Three-year evaluation established a stable hierarchy: EF (R^2=0.72±0.03)>EF′ (0.68± 0.04)>K_c (0.63±0.05)>r_c (0.58±0.06), with EF achieving metric excellence (R^2=0.70-0.74; RRMSE=23.2%-24.1%; ε=0.52-0.54; MAE=0.46-0.47 mm) under greenhouse microclimate conditions (VPD=1.2-2.8 kPa, PAR=800-1200 μmol/(m·s). These results demonstrate the EF method's superior robustness for temporal upscaling applications in greenhouse systems, particularly under high radiative loads.

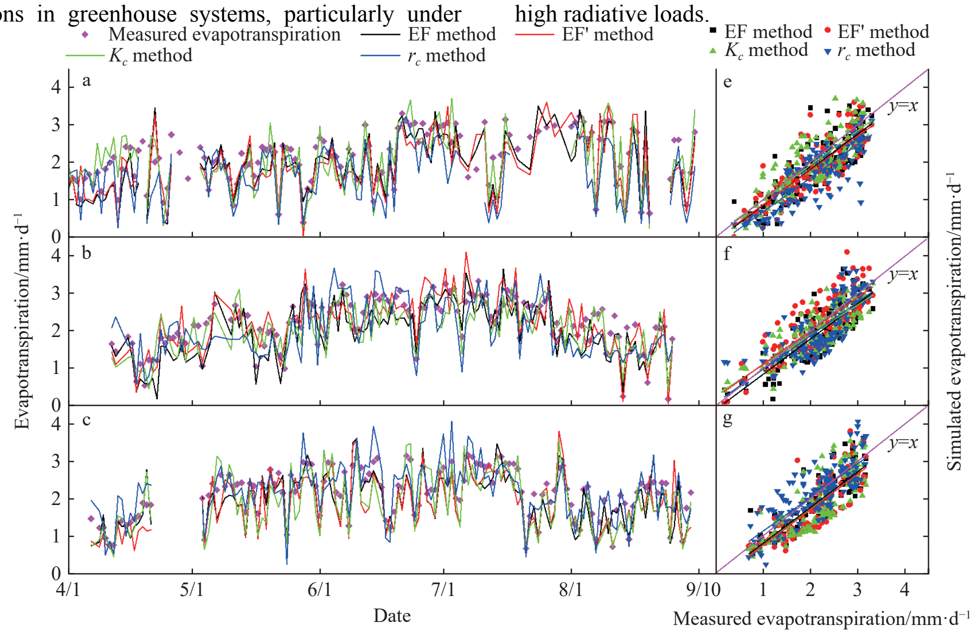

Note: Subfigures a, b, and c show daily simulation results for 2018, 2020, and 2021, respectively; subfigures e, f, and g present simulation results for the corresponding years.

Figure 9 Comparison between simulated and measured evapotranspiration at optimal temporal scaling windows using four methods

Table 2 Simulation results of optimal expansion time of four methods

Year	Method	Linear regression equation	R^2	RRMSE	ε	MAE/mm	N
2018	EF method	y=0.95x–0.10	0.72	23.47%	0.54	0.46	130
	EF′ method	y=0.91x–0.05	0.70	23.82%	0.53	0.47	130
	K_c method	y=0.92x+0.07	0.69	23.97%	0.48	0.48	124
	r_c method	y=0.90x–0.22	0.70	28.07%	0.47	0.56	124
2020	EF method	y=0.94x–0.10	0.70	23.23%	0.52	0.47	131
	EF′ method	y=0.89x+0.22	0.64	23.72%	0.52	0.47	131
	K_c method	y=0.80x+0.28	0.67	24.28%	0.48	0.48	131
	r_c method	y=0.89x+0.08	0.62	27.19%	0.47	0.54	131
2021	EF method	y=0.95x–0.12	0.74	24.11%	0.54	0.46	135
	EF′ method	y=0.95x–0.18	0.69	24.61%	0.52	0.47	135
	K_c method	y=0.97x–0.18	0.67	25.25%	0.49	0.49	135
	r_c method	y=0.90x+0.26	0.64	29.28%	0.47	0.56	135

Note: x represents the measured ET and y represents the simulated ET, R^2 is the determination coefficient, RRMSE is the relative root mean square error, ε is the efficiency coefficient, MAE is the mean absolute error, N is the number of samples.

3.6 Daily to the entire growth period evapotranspiration upscaling

Table 3 lists the entire growth period ET upscaling performance across phenological stages from 2018 to 2021, which revealed systematic methodology biases. All four methods consistently underestimated entire growth period ET when using shoot growth, flowering and fruit setting, and maturity stage typical days, with K_c methodology demonstrating phase dependent divergence overestimating ET during 2018 and 2020 fruit expansion by 12.8%±3.2%, yet underestimating by 9.7% in 2021. Three-year relative errors ranged: EF (11.40%-14.62%), EF′ (12.96%-15.64%), K_c (15.38%-18.51%), and r_c (19.12%-23.78%), establishing a consistent performance hierarchy: EF>EF′>K_c>r_c. Fruit expansion stage EF method achieved superior accuracy (MAE=–33.00 mm, RE=–11.40%; p<0.01 vs. other stages), demonstrating the highest reliability for entire growth period ET temporal integration under greenhouse conditions.

Table 3 Evapotranspiration improvement results from day to entire growth period in 2018, 2020, and 2021

Growing stage	Method	2018				2020				2021			
		Simulated ET/mm	Actual ET/mm	Error/ mm	MAE	Simulated ET/mm	Actual ET/mm	Error/ mm	MAE	Simulated ET/mm	Actual ET/mm	Error/ mm	MAE
Shoot growth stage	EF method	230.68		–58.51	20.23%	233.22		–56.16	19.41%	230.86		–62.98	21.43%
	EF′ method	228.28		–60.91	21.06%	238.11		–51.27	17.72%	224.69		–69.15	23.53%
	K_c method	360.26		71.07	24.58%	359.78		70.40	24.33%	210.38		–83.46	28.40%
	r_c method	193.47		–95.72	33.10%	202.25		–87.13	30.11%	214.30		–79.54	27.07%
Flowering and fruit setting period	EF method	240.92		–48.27	16.69%	239.37		–50.01	17.28%	246.95		–46.89	15.96%
	EF′ method	243.58		–45.61	15.77%	244.57		–44.81	15.48%	241.75		–52.09	17.73%
	K_c method	339.29		50.10	17.32%	334.38		45.00	15.55%	226.59		-67.25	22.89%
	r_c method	200.85	289.19	–88.34	30.55%	231.20	289.38	–58.18	20.10%	222.25	293.84	–71.59	24.36%
Fruit expansion period	EF method	253.88		–35.31	12.21%	256.38		–33.00	11.40%	250.87		–42.97	14.62%
	EF′ method	251.70		–37.49	12.96%	250.18		–39.20	13.55%	247.87		–45.97	15.64%
	K_c method	333.66		44.47	15.38%	331.85		42.47	14.68%	239.46		–54.38	18.51%
	r_c method	220.42		–68.77	23.78%	234.06		–55.32	19.12%	234.98		–58.86	20.03%
Maturity stage	EF method	210.49		–78.70	27.21%	245.13		–44.25	15.29%	235.18		–58.66	19.96%
	EF′ method	217.93		–71.26	24.64%	244.33		–45.05	15.57%	240.47		–53.37	18.16%
	K_c method	344.36		55.17	19.08%	341.19		51.81	17.90%	233.96		–59.88	20.38%
	r_c method	191.99		–97.20	33.61%	230.74		–58.64	20.26%	213.49		–80.35	27.35%

Note: Negative values indicate underestimation. The fruit expansion stage showed significantly lower errors (p<0.05, ANOVA) compared to other stages.

Table 4 compares evapotranspiration temporal upscaling performance of the four methods, demonstrating progressive improvement in accuracy with temporal upscaling. For instantaneous-to-daily upscaling, RRMSE values measured 23.21% (EF), 23.26% (EF′), 23.92% (K_c), and 27.55% (r_c), decreasing significantly (Δ=10.37%, 9.14%, 7.62%, 6.49%) during daily to entire growth period upscaling to 12.84% (EF), 14.12% (EF′), 16.30% (K_c), 21.06% (r_c). EF method achieved maximum error reduction, while K_c showed greatest ARE improvement (Δ=3.39%). Initial ARE values (instantaneous-daily) spanned 19.40% (EF), 20.22% (EF′), 22.00% (K_c), 24.78% (r_c), systematically decreasing to 16.64% (EF), 16.33% (EF′), 18.59% (K_c), 24.00% (r_c) at growth-period scale, confirming temporal aggregation's error mitigation effects. This study identified the EF method employing growth stage averaging during fruit expansion as optimal for daily-to-growth-period ET upscaling, contrasting with Liu et al.'s K_c-based superiority in winter wheat systems[32]. The methodological differences originate from Liu's implementation of daily interpolation versus this novel phenological-stage averaging protocol, which mitigates sampling bias in daily representation.

Table 4 Comparison of evapotranspiration upscaled at different time scales

Method	RMSE/mm		RRMSE		ARE		MAE/mm	
	Instant to day	Day to entire growth period	Instant to day	Day to entire growth period	Instant to day	Day to entire growth period	Instant to day	Day to entire growth period
EF method	0.51	37.34	23.21%	12.84%	23.21%	12.84%	0.45	37.09
EF′ method	0.51	41.06	23.26%	14.12%	23.26%	14.12%	0.46	40.89
K_c method	0.53	47.40	23.92%	16.30%	23.92%	16.30%	0.48	47.11
r_c method	0.60	61.24	27.55%	21.06%	27.55%	21.06%	0.57	60.98

Note: RRMSE represents the relative root mean square error and ARE represents the absolute relative error.

4 Discussion

4.1 Selection and parameterization of temporal upscaling factors

This study demonstrates that during instantaneous-to-daily ET upscaling, the key parameters (EF, EF′, K_c, and r_c) exhibited characteristic U-shaped diurnal variations with pronounced midday stability. These findings align with Yan et al.[22] but contrast with Zhang et al.[27], who reported minimal EF and K_c fluctuations and progressively increasing r_c in summer maize systems. Such discrepancies are primarily attributable to fundamental micro-climatic differences between greenhouse and open-field conditions. As semi-closed ecosystems, greenhouses feature limited air convection, elevated humidity, and higher temperatures, which collectively alter ET parameter dynamics[11,43]. Additionally, low solar radiation and weak sap flow during morning and evening hours reduce available energy and amplify sensor measurement errors, potentially inflating parameter values[44,45]. Li et al.[12] similarly observed an upward intra-day trend in r_c for rice, reinforcing stomatal regulation's dominant role, a mechanism that Yang et al.[46] linked to the synchronous variations of EF, EF′, and r_c due to their shared dependence on stomatal behavior. Grapevine exhibited stable midday values of EF (0.5), EF′ (0.5), K_c (0.8), and r_c (200 s/m), contrasting with tea plantation parameters (EF: 0.6, EF′: 0.6, K_c: 1.0, r_c: 100 s/m) reported by Yan et al.[22]. Soil mulching effectively suppressed evaporation, reducing EF, EF′, and K_c by 20%-30% compared to unmulched conditions, while elevated r_c levels (250-300 s/m) likely resulted from restricted air circulation (85% relative humidity) in the greenhouse. Comparative analysis reveals ecosystem specific parameterization: rice systems maintain higher EF (0.8) and K_c (1.2)[12], and summer maize shows intermediate values (EF: 0.7, K_c: 0.9)[27], both exceeding our observations by 15%-20%, while semi-arid sorghum/grass systems[24] exhibit significantly lower EF (0.3). This continuum underscores strong microenvironmental regulation of ET parameters across irrigated greenhouse and rainfed field conditions.

4.2 Optimal time window for ET upscaling

This investigation confirms the critical influence of temporal window selection on ET simulation accuracy, with optimal upscaling performance consistently clustered around solar noon (11:00–12:30 LST) across methodologies, aligning with the greenhouse observations by Chen et al.[24] The temporal analysis identified minimal parameter variability from 08:00 to 16:00, a broader window than previous crop-specific observations: rice systems showed K_c stabilization from 09:00-15:00 and r_c from 08:00-12:00[12], while winter wheat exhibited reduced EF and K_c fluctuations from 10:00–15:00[47]. These temporal discrepancies originate from: 1) agroecosystem heterogeneity in vegetation cover and hydroclimatic conditions[48-50]; 2) K_c sensitivity to topsoil moisture dynamics[36]; and 3) r_c's microenvironmental dependence[51], particularly the divergence in environmental forcing between greenhouse and field conditions.

Comparative analyses reveal significant spatiotemporal heterogeneity in optimization windows. Yan et al.[22] identified 11:00–14:00 LST for tea plantations (humid subtropical; $\Delta_{SolarNoon}$=+23 min) versus winter wheat (continental; $\Delta_{SolarNoon}$=–17 min). Liu et al.[28] reported physiology-driven patterns in winter wheat: 14:00–15:00 LST for K_c and EF versus 10:00–11:00 LST for r_c. Zhang et al.[27] showed afternoon optimization peaks (14:00-16:00 LST) correlating with crop-specific stomatal regulation dynamics. These geographical disparities primarily stem from longitudinal solar noon variations (Δ=1.2-2.1 h) and greenhouse-specific microenvironmental modifications (RH=65%-85% vs. field 45%-60%). Notably, despite optimal window selection, a systematic ET underestimation (4.8%-7.2%) persisted across all methods. This bias echoes the radiative transfer model limitations noted by Jiang et al.[25], while such underestimation can be exacerbated by meteorological disturbances like cloud cover (index>0.3 in Nassar et al.[26]). Its persistence under the controlled clear-sky conditions suggests an inherent model structural bias within the instantaneous ET estimation chain.

4.3 ET upscaling methods in greenhouse conditions

This investigation confirms the superior performance of the EF method for temporal ET upscaling over EF′, K_c, and r_c approaches, consistent with findings by Yan et al.[22] in tea and wheat systems. In contrast, Chen et al.[24] reported the superiority of EF′ in wheat and maize systems, a discrepancy primarily attributable to: 1) inaccuracies in soil heat flux measurement (RMSE=12-18 W/m^2) due to installation depth effects on thermal conductivity[52]; and 2) surface soil moisture modulation (θ_v=0.25-0.35 m^3/m^3) altering soil heat flux dynamics[22]. Furthermore, while Colaizzi[13] observed K_c dominance in semi-arid Texan crops (ET_0=5-7 mm/d), its efficacy declined in this irrigated system (ET_0=3.2-4.1 mm/d), associated with diminished soil water stress (SWP>–0.5 MPa) and discrepancies in aerodynamic roughness between greenhouse and natural environments, particularly challenging for Penman-Monteith applications in semi-arid regions [46].

Comparative analysis reveals fundamental differences in optimal ET upscaling methods between greenhouse and open-field environments, driven by distinct microclimates and crop physiological responses. Three key factors explain this divergence: 1) Microclimate modification effects: greenhouse conditions alter energy partitioning, with reduced turbulent mixing enhancing the relative importance of radiative components[11]. While field studies indicate strong dependence on aerodynamic resistance[46], this study's results show EF stability (SD=0.08–0.21) stems from suppressed vapor pressure deficit fluctuations, supporting Jiang et al.[25] that EF methods excel under constrained atmospheric coupling. 2) Soil-plant-atmosphere continuum differences: mulch-covered greenhouse soils exhibited minimal evaporation[36], validating EF's omission of soil heat flux (G), whereas field studies require G consideration due to bare soil exposure[13]. This study's canopy resistance values (256.3±72.3 s/m) were 2-3 times higher than field reports[7], explaining the reduced performance of r_c-based methods in greenhouses. 3) Temporal dynamics variation: the 08:00–16:00 parameter stability window in greenhouses was 2-3 h longer than in field observations[53], attributed to attenuated radiation extremes, buffered temperature fluctuations, and higher humidity persistence (Figure 1). These findings align with Nassar et al.[26] on greenhouse systems but contrast with open-field recommendations.

4.4 Advantages, limitations, and future perspectives of the current study

The present study provides a robust framework for evapotranspiration (ET) upscaling in solar greenhouses, employing physically based models (EF, EF′, K_c, and r_c methods) validated with three years of high-resolution sap flow and microclimate data. Key strengths include: 1) Biological interpretability: Direct measurement of canopy resistance (r_c) and soil-plant-atmosphere interactions ensures physiological relevance, unlike purely data-driven approaches. 2) Practical applicability: The EF method's minimal data requirements (Rn and λET) make it practical for greenhouse irrigation management without complex computational infrastructure. 3) Temporal stability: Demonstrated consistency of key parameters (e.g., EF stability from 08:00-16:00) provides reliable inputs for irrigation scheduling.

In a greenhouse environment, evapotranspiration not only reflects crop water consumption but also exhibits strong coupling relationships with environmental factors such as temperature, humidity, light, and CO_2 concentration. When light intensity suddenly increases, the crop transpiration rate rapidly rises; if irrigation response is delayed, water stress may occur. Conversely, irrigation scheduled at fixed intervals may lead to water waste on cloudy days. By upscaling evapotranspiration data and integrating it into the environmental control system, coordinated regulation based on actual crop demand can be achieved. Furthermore, by selecting an appropriate upscaling method and optimal observation period, the cumulative water consumption of crops can be accurately derived from instantaneous monitoring data, thereby guiding irrigation amounts at different growth stages and providing a scientific basis for precision irrigation in greenhouses.

While effective, the current approach does not leverage modern machine learning (ML) techniques that could address inherent constraints. The study assumes constant relationships through static parameterization, whereas ML models like random forest[4] could dynamically optimize parameters based on real-time microclimate data. Deep learning architectures[54] may better capture in ET dynamics, which are oversimplified in current resistance-based models. Unlike the current single-site validation, hybrid models[25] could integrate multi-location greenhouse data to improve generalizability, as demonstrated for open-field ET upscaling. To bridge these gaps, future research should pursue two synergistic directions: First, combining the physical foundations of EF and K_c approaches with ML methodologies; second, constructing hybrid physical-ML frameworks that balance interpretability with the predictive performance of state-of-the-art algorithms.

5 Conclusions

This three-year study (2018, 2020, 2021) evaluated four evapotranspiration (ET) upscaling methods EF, EF′, K_c, and r_c for drip-irrigated grapevines in Northeast China's cold region greenhouses. Key parameters remained stable from 08:00-16:00 (SD ranges: EF: 0.08-0.21, EF′: 0.08-0.19, K_c: 0.10-0.18, r_c: 41.43-137.72 s/m). Optimal instantaneous-to-daily upscaling windows occurred between 11:00-13:30 LST. The EF method consistently outperformed other methods across both upscaling procedures (EF>EF′>K_c>r_c). For instantaneous-to-daily upscaling, it achieved highest accuracy (R^2=0.72, RRMSE=23.23%, MAE=0.46 mm). For daily-to-growth-period upscaling, the fruit expansion stage yielded optimal results, with the EF method again superior (RE: 11.40%-14.62%). Upscaling accuracy improved with temporal scale extension (EF method RRMSE reduced from 23.21% to 12.84%). Therefore, the EF method is recommended as the optimal approach for ET temporal upscaling in greenhouse grape systems.

These findings support implementing hourly precision water management in greenhouse grape cultivation. However, several limitations warrant consideration: the study was conducted under clear-sky conditions in a single greenhouse system, requiring further validation for cloudy conditions and diverse greenhouse designs; systematic underestimation persisted across methods, suggesting inherent biases in instantaneous ET estimation that merit investigation through model refinement; and the EF method's reliance on net radiation measurements may limit adoption in greenhouses lacking sophisticated instrumentation. Future research should explore hybrid physical-machine learning approaches to reduce systematic biases and improve generalizability across diverse greenhouse environments.

Acknowledgements

This work was supported by the National Natural Science Foundation of China (Grant No. 51709174) and the General Project of Liaoning Provincial Department of Education (Grant No. JYTMS20231272 and LJKMZ20220749).

[References]

[1] Allen R G, Pereira L S, Raes D, Smith M. Crop evapotranspiration-guidelines for computing crop water requirements-FAO irrigation and drainage paper 56. Rome: FAO, 1998.

[2] Dai J J, Zhang X P, Luo Z D, Wang R, Liu Z L, et al. Variation of the stable isotopes of water in the soil-plant-atmosphere continuum of a cinnamomum camphora woodland in the East Asian monsoon region. Journal of Hydrology, 2020; 589: 125199.

[3] Nyolei D, Diels J, Mbilinyi B, Mbungu W, van Griensven A. Evapotranspiration simulation from a sparsely vegetated agricultural field in a semi-arid agro-ecosystem using Penman-Monteith models. Agricultural and Forest Meteorology, 2021; 303: 108370.

[4] Wang Z C, Pan X, Ding X, Guluzade R, Yang Z, Yuan J, et al. Intercomparison of temporal upscaling strategies for daily evapotranspiration estimation from the perspective of land surface temperature. Journal of Hydrology, 2025; 660(B): 133461.

[5] Kumar U, Sahoo B, Chatterjee C, Raghuwanshi N S. Evaluation of

simplified surface energy balance index (s-sebi) method for estimating actual evapotranspiration in Kangsabati Reservoir command using landsat 8 imagery. Journal of the Indian Society of Remote Sensing, 2020; 48: 1421–1432.

[6] Shirmohammadi-Aliakbarkhani Z, Saberali S F. Evaluating of eight evapotranspiration estimation methods in arid regions of Iran. Agricultural Water Management, 2020; 239: 106243.

[7] Yang Y, Chen R S, Song Y X, Han C T, Liu J F, Liu Z W. Sensitivity of potential evapotranspiration to meteorological factors and their elevational gradients in the Qilian Mountains, northwestern China. Journal of Hydrology, 2019; 568: 147–159.

[8] Wang C, Jiang Y C, Bai Y K, Wang T L. Numerical study on static properties and failure mechanisms of landing assembled Chinese solar greenhouses. Computers and Electronics in Agriculture, 2021; 188: 106347.

[9] Jackson R D, Hatfield J L, Reginato R J, Idso S B, Pinter Jr P J. Estimation of daily evapotranspiration from one time-of-day measurements. Agricultural Water Management, 1983; 7: 351–362.

[10] Zhang B Z, Xu D, Liu Y, Li F S, Cai J B, Du L J. Multi-scale evapotranspiration of summer maize and the controlling meteorological factors in north China. Agricultural and Forest Meteorology, 2016; 216: 1–12.

[11] Gong X W, Liu H, Sun J S, Zhang H, Ma X J, Wang W N. Variation of evapotranspiration in different spatial scales for solar greenhouse tomato and its controlling meteorological factors. Transactions of the Chinese Society of Agricultural Engineering, 2017; 33(8): 166–175. (in Chinese)

[12] Li Y, Liu X Y, Xu Z W, Peng Y H, Xu J Z. Comparative analysis of different temporal up-scaling methods for evapotranspiration applied to water-saving irrigated paddy fields. Transactions of the Chinese Society of Agricultural Engineering, 2021; 37(21): 90–99. (in Chinese)

[13] Colaizzi P D, Evett S R, Howell T A, Tolk J A. Comparison of five models to scale daily evapotranspiration from one-time-of-day measurements. Transactions of the ASABE, 2006; 49(5): 1409–1417.

[14] Shuttleworth W, Gurney R, Hsu A, Ormsby J. Fife: the variation in energy partition at surface flux sites. IAHS Publications, 1989; 186: 523–534.

[15] Sugita M, Brutsaert W. Daily evaporation over a region from lower boundary layer profiles measured with radiosondes. Water Resources Research, 1991; 27(5): 747–752.

[16] Chemin Y, Alexandridis T. Improving spatial resolution of ET seasonal for irrigated rice in Zhanghe, China. In: 22nd Asian Conference on Remote Sensing, Singapore: CRISP, 2001.

[17] Farah H O, Bastiaanssen W G M, Feddes R A. Evaluation of the temporal variability of the evaporation fraction in a tropical watershed. International Journal of Applied Earth Observation and Geoinformation, 2004; 5(2): 129–140.

[18] Malek E, Bingham G E, McCurdy G D. Continuous measurement of aerodynamic and alfalfa canopy resistances using the Bowen ratio-energy balance and Penman-Monteith methods. Boundary-Layer Meteorology, 1992; 59: 187–194.

[19] Tang R, Li Z L, Sun X M, Bi Y Y. Temporal upscaling of instantaneous evapotranspiration on clear - sky days using the constant reference evaporation fraction method with fixed or variable surface resistances at two cropland sites. Journal of Geophysical Research: Atmospheres, 2017; 122(2): 784–801.

[20] Chen R N, Liu X J, Liu L Y. Improved GPP upscaling from instantaneous measurements to daily sums using the light-use-efficiency-based model. Agricultural and Forest Meteorology, 2025; 368: 110529.

[21] Katimbo A, Rudnick D R, Liang W Z, DeJonge K C, Lo T H, Franz T E, et al. Two source energy balance maize evapotranspiration estimates using close-canopy mobile infrared sensors and upscaling methods under variable water stress conditions. Agricultural Water Management, 2022; 274: 107972.

[22] Yan H F, Li M, Zhang C, Zhang J Y, Wang G Q, Yu J J, et al. Comparison of evapotranspiration upscaling methods from instantaneous to daytime scale for tea and wheat in southeast China. Agricultural Water Management, 2022; 264: 107464.

[23] Yang D N, Yang S S, Huang J J, Zhang S Y, Zhang S, Zhang J H, et al. Improving time upscaling of instantaneous evapotranspiration based on machine learning models. Big Earth Data, 2025; 9(1): 127–154.

[24] Chen H, Yang D W, Lyu H F. Comparison of temporal extrapolation methods for evapotranspiration over variant underlying croplands. Transactions of the Chinese Society of Agricultural Engineering, 2013; 29(6): 73–81. (in Chinese)

[25] Jiang L, Zhang B Z, Han S J, Chen H, Wei Z. Upscaling evapotranspiration from the instantaneous to the daily time scale: assessing six methods including an optimized coefficient based on worldwide eddy covariance flux network. Journal of Hydrology, 2021; 596: 126135.

[26] Nassar A, Torres-Rua A, Kustas W, Alfieri J, Hipps L, Prueger J, et al. Assessing daily evapotranspiration methodologies from one-time-of-day sUAS and EC information in the GRAPEX project. Remote Sensing, 2021; 13(15): 2887.

[27] Zhang B Z, Chen H, Xu D, Li F S. Methods to estimate daily evapotranspiration from hourly evapotranspiration. Biosystems Engineering, 2017; 153: 129–139.

[28] Liu G S, Liu Y, Xu D. Comparison of evapotranspiration temporal scaling methods based on lysimeter measurements. Journal of Remote Sensing, 2011; 15(2): 270–280. (in Chinese)

[29] Gao X, Mei X R, Zhang J S, Cai J F, Gu F X, Hao W P, et al. Comparison of three modified models in evapotranspiration and its components over a rainfed spring maize cropland on the loess plateau, China. Agricultural and Forest Meteorology, 2023; 330: 109322.

[30] Wang J X, Cai Y H, Gao X D, Zhou Y Q, Wu P T, Zhao X N. Modeling the dynamics of evapotranspiration of wolfberry (Lycium barbarum L.) under different cultivation methods on the Tibetan Plateau. Journal of Hydrology (Amsterdam), 2024; 639: 131537.

[31] Cui N B, He Z L, Jiang S Z, Wang M J, Yu X Y, Zhao L, et al. Inter-comparison of the Penman-Monteith type model in modeling evapotranspiration and its components in an orchard plantation of southwest China. Agricultural Water Management, 2023; 289: 108541.

[32] Wei X G, Zheng S Y, Chen D Y, Qiu L C. Estimation of evapotranspiration and its components of drip-irrigated grapevine under greenhouse conditions in cold Northeast China. Irrigation Science, 2025; 43: 755–772.

[33] Fu S N, Wei X G, Wang T L, Bai Y K. Effects of different water and fertilizer treatments on grapevine sap flow and water consumption characteristics. Scientia Horticulturae, 2022; 304: 111317.

[34] Zhao P, Li S E, Li F S, Du T S, Tong L, Kang S Z. Comparison of dual crop coefficient method and Shuttleworth–Wallace model in evapotranspiration partitioning in a vineyard of northwest China. Agricultural Water Management, 2015; 160: 41–56.

[35] Allen R G, Tasumi M, Trezza R. Satellite-based energy balance for mapping evapotranspiration with internalized calibration (metric)—method. Journal of Irrigation and Drainage Engineering, 2007; 133: 380–394.

[36] Zhang Y Q, Wang J D, Gong S H, Xu D, Sui J, Wu Z D. Analysis of water saving and yield increasing mechanism in maize field with drip irrigation under film mulching based on transpiration estimated by sap flow meter. Transactions of the Chinese Society of Agricultural Engineering, 2018; 34(21): 89–97.

[37] Zheng S Y, Cui N B, Wei X G, Wang T L, Bai Y K, Pei D J, et al. Dynamics, plant physiological and environmental controls of energy exchange in a grapevine greenhouse in northeast China. Journal of Hydrology, 2024; 637: 131395.

[38] Pei D J, Wei X G, Bai Y K, Wang C, Liu Y, Jiang S Y. Path analysis of the main control factors of transpiration in greenhouse, drip-irrigated grapes in cold areas of northeast China. Water, 2022; 14(22): 3764.

[39] Tasumi M, Allen R G, Trezza R, Wright J L. Satellite-based energy balance to assess within-population variance of crop coefficient curves. Journal of Irrigation and Drainage Engineering, 2005; 131: 94.

[40] McAdams W H. Heat transmission (3rd ed.). 1954. doi: 10.1126/science.120.3128.984

[41] Zheng S Y, Wang T L, Wei X G. Estimating grapevine transpiration in greenhouse with three different methods in a Penman–Monteith model in northeast China. Irrigation Science, 2022; 40: 13–27.

[42] Wei X G, Wu L L, Ge D, Yao M Z, Bai Y K. Prediction of the maturity of greenhouse grapes based on imaging technology. Plant Phenomics, 2022; 2022: 9753427.

[43] Xia H M, Li A N, Zhao W, Bian J H. Review of temporal scale expansion for evapotranspiration retrieved by remote sensing data. Transactions of the Chinese Society of Agricultural Engineering, 2015; 31(24): 162–173. (in Chinese)

[44] Yan H F, Zhang C, Gerrits M C, Acquah S J, Zhang H N, Wu H M, et al. Parametrization of aerodynamic and canopy resistances for methoding evapotranspiration of greenhouse cucumber. Agricultural and Forest

Meteorology, 2018; 262: 370–378.

[45] Qiang X M, Cai H J, Zhou X G, Wang J. Experimental study on alfalfa's canopy resistance and its variation under reference condition. Agricultural Research in the Arid Areas, 2009; 27: 107–111. (in Chinese)

[46] Yang D W, Chen H, Lei H M. Analysis of the diurnal pattern of evaporation fraction and its controlling factors over croplands in the northern China. Journal of Integrative Agriculture, 2013; 12(8): 1316–1329.

[47] Hua J C, Zhu Y H, Wang Z L, Lyu H S. Spatiotemporal variation of crop coefficient of winter wheat in Huaibei Plain. Journal of Irrigation and Drainage, 2021; 40(2): 118–124. (in Chinese)

[48] Chen Z J, Zhu Z C, Sun S J, Wang Q Y, Su T Y, Fu Y J. Estimation of daily evapotranspiration and crop coefficient of maize under mulched drip irrigation by stacking ensemble learning mode. Transactions of the Chinese Society of Agricultural Engineering, 2021; 37(5): 95–104. (in Chinese)

[49] Higuchi A, Kondoh A, Kishi S. Relationship among the surface albedo, spectral reflectance of canopy, and evaporation fraction at grassland and paddy field. Advances in Space Research, 2000; 26(7): 1043–1046.

[50] Kurc S A, Small E E. Dynamics of evapotranspiration in semiarid grassland and shrubland ecosystems during the summer monsoon season, central New Mexico. Water Resources Research, 2004; 40(9): 2004WR003068.

[51] Liu X Y, Gao M Y, Zhou X Y, Xu J Z. Enforcing energy balance closure by evaporation ratio method and its effect on evapotranspiration estimation of paddy fields. Transactions of the Chinese Society of Agricultural Engineering, 2021; 37(11): 121–130. (in Chinese)

[52] Xing Z, Qiao Z Y, Liu G. Measuring error of soil heat flux plate and applicability of Philip's equation for modification. Acta Pedologica Sinica, 2020; 57(1): 92–99. (in Chinese)

[53] Liu X Y, Xu J Z, Zhou X Y, Wang W G, Yang S H. Evaporation fraction and its application in estimating daily evapotranspiration of water-saving irrigated rice field. Journal of Hydrology, 2020; 584: 124317.

[54] Rong Y, Wang W S, Wu P J, Wang P, Zhang C L, Wang C Z, et al. A novel hybrid deep learning framework for evaluating field evapotranspiration considering the impact of soil salinity. Water Resources Research, 2024; 60(9): e2023WR036809.